Pergamon

Int. J. Solids Structures Vol. 33, No. 15, pp. 2193–2211, 1996

0020–7683/96 $15.00 + .00

0020–7683(95)00126–3

TRACTION AND CONTACT PROBLEMS FOR AN ANISOTROPIC MEDIUM WITH A CYLINDRICAL BOREHOLE

R. K. N. D. RAJAPAKSE† and D. GROSS
Institute of Mechanics, TH Darmstadt, 64289 Darmstadt, Germany

(*Received* 13 *September* 1994; *in revised form* 15 *May* 1995)

Abstract—General solutions for axisymmetric displacements and stresses of a transversely isotropic annular cylinder of infinite length are derived by using Fourier integral transforms. These general solutions are used to solve boundary-value problems corresponding to radial and tangential tractions applied over a finite segment of the surface of a cylindrical borehole in an infinite medium. Contact problems involving a rigid cylinder with a radial misfit and a rigid cylinder subjected to an axial load are analysed by numerically solving the governing integral equations. The accuracy of present solutions is confirmed by comparison with the solutions reported by Parnes [(1993) Applied tractions on the surface of an infinite cylindrical bore. *Int. J. Solids Structures* **19**, 165–177] for radial tractions applied to a borehole in an isotropic medium. Selected numerical results for displacements and stresses are presented to portray the influence of material anisotropy, type of loading and the aspect ratio of a rigid cylinder on the elastic fields. It is found that the axial stiffness of a rigid cylinder bonded to a borehole can be used to approximate the stiffness of a rigid cylinder in an elastic half space. The relevance of present analysis to the solution of problems encountered in geomechanics and mechanics of composite materials is discussed. Copyright © 1996 Elsevier Science Ltd.

INTRODUCTION

The development of analytical and computational methods for stress analysis of an anisotropic medium with a cylindrical borehole is useful to the modelling of a variety of problems encountered in geomechanics and mechanics of composite materials. For example, theoretical modelling of borehole stress fields, in situ testing devices such as pressuremeter, massive bore-hole plugs, fibre pull-out experiments, residual stresses due to thermal mismatch strains between a fibre and a matrix, and the interaction between broken or debonded fibres and a matrix material involve the study of axisymmetric response of an elastic medium with a cylindrical borehole under surface tractions or the analysis of contact problems involving a rigid or a flexible cylinder bonded to a borehole. A review of existing literature reveals that solutions to problems related to tractions applied over a finite segment of the surface of a cylindrical borehole in an infinite isotropic elastic medium are available (Jordan, 1962; Parnes, 1983 a and b; Parnes, 1984; Parnes, 1986). In addition, Muki and Sternberg (1969) considered the axial load transfer from an infinite cylindrical fibre bonded to an infinite isotropic elastic medium. It is well known that the presence of material anisotropy strongly influences the response of an elastic medium (Green and Zerna, 1968). Given the fact that geomaterials and fibre-reinforced composite materials are anisotropic, it is important that a realistic form of anisotropy be included in the analysis of boundary-value problems involving such materials. Among a variety of material anisotropy models available, the transversely isotropic elastic material model (Lekhnitskii, 1963) can be considered as a suitable model for geomaterials (Gibson, 1972) and fibre-reinforced composites (Sendeckyj, 1974).

In view of the relevance of stress analysis of a transversely isotropic elastic medium with a cylindrical borehole to a number of problems encountered in geomechanics and mechanics of composite materials, the present paper examines a selected set of boundary-value problems involving such a medium. Initially a set of general solutions for displacements and stresses of a transversely isotropic annular cylinder of finite thickness and

†Permanent address and correspondence: Department of Civil and Geological Engineering, University of Manitoba, Winnipeg, Canada R3T 5V6.

infinite length are derived by applying Fourier integral transforms with respect to the vertical coordinate. General solutions corresponding to a solid cylinder and an infinite medium with a cylindrical borehole are obtained as limiting cases. Boundary-value problems corresponding to uniform radial and shear tractions applied over a finite segment of the surface of a cylindrical borehole in an unbounded transversely isotropic medium are solved. Solutions for radial and tangential ring loads are also presented. Contact problems related to a finite rigid cylinder subjected to an axial load and a cylinder with a radial misfit are formulated in terms of a pair of singular integral equations. These integral equations are solved numerically by replacing the singular kernels with appropriate non-singular kernels. Selected numerical results are presented to demonstrate the influence of material anisotropy and the type of loading on stresses and displacements due to tractions applied to a borehole surface. Contact stresses and stiffness of a rigid cylindrical inclusion subjected to an axial load and an inclusion with a radial mis-fit are also presented.

GOVERNING EQUATIONS AND GENERAL SOLUTIONS

Consider an unbounded transversely isotropic elastic medium with a cylindrical borehole of radius a. A cylindrical polar coordinate system (r, θ, z) and a Cartesian coordinate system (x, y, z) are chosen such that the axis of elastic symmetry is parallel to the axis of the borehole (Fig. 1). The mechanical response of a transversely isotropic elastic medium is governed by five elastic moduli denoted by c_{11}, c_{12}, c_{13}, c_{33} and c_{44} which relate the stresses and strains referred to a cylindrical polar coordinate system in the following manner (Lekhnitskii, 1963).

$$\sigma_{rr} = c_{11}\varepsilon_{rr} + c_{12}\varepsilon_{\theta\theta} + c_{13}\varepsilon_{zz} \tag{1a}$$

$$\sigma_{\theta\theta} = c_{12}\varepsilon_{rr} + c_{11}\varepsilon_{\theta\theta} + c_{13}\varepsilon_{zz} \tag{1b}$$

$$\sigma_{zz} = c_{13}\varepsilon_{rr} + c_{13}\varepsilon_{\theta\theta} + c_{33}\varepsilon_{zz} \tag{1c}$$

$$\sigma_{rz} = 2c_{44}\varepsilon_{rz}. \tag{1d}$$

In writing eqns (1), it is assumed that the deformation field is axially symmetric and the shear strains $\varepsilon_{r\theta} = \varepsilon_{z\theta} \equiv 0$ and the shear stresses $\sigma_{r\theta} = \sigma_{\theta z} \equiv 0$. Positive definiteness of strain energy requires that $c_{11} > 0$, $c_{33} > 0$, $c_{44} > 0$, $c_{11} > |c_{12}|$ and $(c_{11}c_{33} - 2c_{13}^2 + c_{12}c_{33}) > 0$ (Eubanks and Sternberg, 1954).

In the absence of body forces, the displacement and stress fields in a transversely isotropic linear elastic material, subjected to a state of axisymmetric deformations about

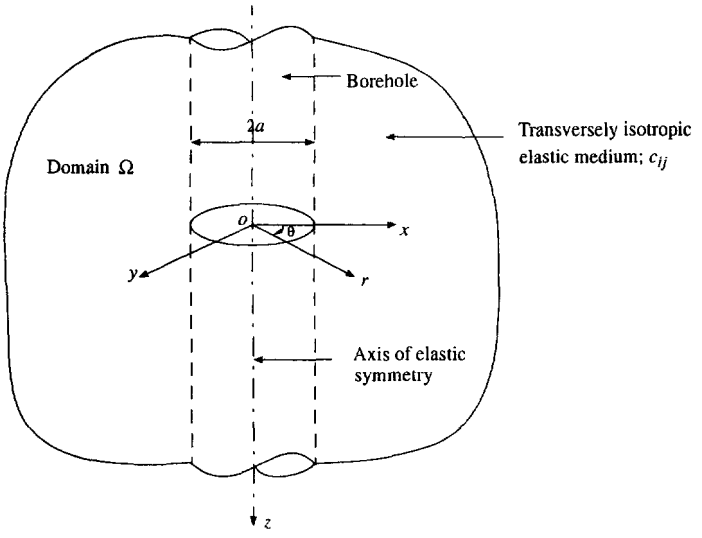

Fig. 1. Borehole geometry and coordinate systems.

the axis of elastic symmetry, can be expressed in terms of two potential functions $\phi_j(r,z)$, $j=1,2$ which are solutions of (Green and Zerna, 1968)

$$\left[\frac{\partial^2}{\partial r^2}+\frac{1}{r}\frac{\partial}{\partial r}+\frac{\partial^2}{\partial z_j^2}\right]\phi_j(r,z)=0, \quad j=1,2 \tag{2}$$

where

$$z_j = z/\sqrt{v_j}, \quad j=1,2 \tag{3}$$

and v_1 and v_2 are the roots of the equation

$$c_{11}c_{44}v^2+[c_{13}(2c_{44}+c_{13})-c_{11}c_{33}]v+c_{33}c_{44}=0. \tag{4}$$

The roots v_1 and v_2 may be real or complex conjugates depending on the values of the five material constants. Since displacements and stresses must be real, the potential functions ϕ_1 and ϕ_2 are complex conjugates when v_1 and v_2 are complex. In addition, it is necessary to specify that $\mathrm{Re}\,(v_1, v_2) \geqslant 0$.

The displacements in the r- and the z-directions denoted by $u_r(r,z)$ and $u_z(r,z)$ respectively are related to the potential functions $\phi_j(r,z), j=1,2$ in the following manner.

$$u_r = \frac{\partial}{\partial r}(\phi_1+\phi_2) \tag{5a}$$

$$u_z = \frac{\partial}{\partial z}(\omega_1\phi_1+\omega_2\phi_2) \tag{5b}$$

where

$$\omega_j = \frac{c_{11}v_j-c_{44}}{c_{13}+c_{44}}, \quad j=1,2. \tag{6}$$

A representation for relevant stresses in terms of ϕ_1 and ϕ_2 can be obtained from eqns (1) and (5). The potential function representation for displacements given by eqns (2)–(5) is based on the condition that roots v_1 and v_2 of eqn (4) are not equal. A solution to the equal root case can be obtained through a suitable limiting procedure from the solutions corresponding to unequal root case or an alternative potential function representation (Chen, 1966; Wang, 1992).

It is convenient to nondimensionalize all quantities including the coordinates with respect to the radius of a borehole which is hereafter considered as a unit length. Stresses are nondimensionalized with respect to c_{44}. Nondimensional quantities are adopted in the ensuing analysis while retaining all of the foregoing notations for convenience.

In order to derive general solutions for axisymmetric torsionless deformations of an annular cylinder, the solutions for potential functions governed by eqn (2) are expressed in the following Fourier integral form (Sneddon, 1951).

$$\phi_j(r,z) = \frac{1}{\sqrt{2\pi}}\int_{-\infty}^{\infty}\bar{\phi}_j(r,\zeta)e^{-i\zeta z}\,\mathrm{d}\zeta, \quad j=1,2 \tag{7}$$

where $\bar{\phi}_j(r,\zeta)$ denotes the Fourier transform of $\phi_j(r,z)$ with respect to the z-coordinate which is defined as (Sneddon, 1951)

$$\bar{\phi}_j(r,\zeta) = \frac{1}{\sqrt{2\pi}}\int_{-\infty}^{\infty} \phi_j(r,z)e^{i\zeta z}\,dz, \quad j = 1,2. \tag{8}$$

The substitution of eqn (7) in eqn (2) results in the following solution for $\bar{\phi}_j(r,\zeta)$.

$$\bar{\phi}_j(r,\zeta) = A_j(\zeta)I_0(\zeta_j r) + B_j(\zeta)K_0(\zeta_j r) \tag{9}$$

where

$$\zeta_j = |\zeta|\sqrt{v_j}, \quad j = 1,2 \tag{10}$$

and $A_j(\zeta)$ and $B_j(\zeta)$ are arbitrary functions to be determined from the boundary and continuity conditions. In addition, I_n and K_n denote the modified Bessel functions (Abramowitz and Segun, 1965) of the first and the second kind of the order n respectively.

In view of eqns (1), (5) and (9), the general solutions for Fourier transforms of displacements and stresses, denoted by $\bar{u}_i(r,\zeta)$ and $\bar{\sigma}_{ij}(r,\zeta)$ respectively, can be expressed as

$$\bar{u}_r(r,\zeta) = \sum_{j=1}^{2} \zeta_j[A_jI_1(\zeta_j r) - B_jK_1(\zeta_j r)] \tag{11}$$

$$\bar{u}_z(r,\zeta) = -\sum_{j=1}^{2} i\zeta\omega_j[A_jI_0(\zeta_j r) + B_jK_0(\zeta_j r)] \tag{12}$$

$$\bar{\sigma}_{rr}(r,\zeta) = \sum_{j=1}^{2} \{A_j[\lambda_j\zeta_j^2 I_0(\zeta_j r) - \alpha\zeta_j r^{-1}I_1(\zeta_j r)] + B_j[\lambda_j\zeta_j^2 K_0(\zeta_j r) + \alpha r^{-1}\zeta_j K_1(\zeta_j r)]\} \tag{13}$$

$$\bar{\sigma}_{\theta\theta}(r,\zeta) = \sum_{j=1}^{2} \{A_j[(\lambda_j - \alpha)\zeta_j^2 I_0(\zeta_j r) + \alpha\zeta_j r^{-1}I_1(\zeta_j r)] + B_j[(\lambda_j - \alpha)\zeta_j^2 K_0(\zeta_j r) - \alpha r^{-1}\zeta_j K_1(\zeta_j r)]\} \tag{14}$$

$$\bar{\sigma}_{zz}(r,\zeta) = -\sum_{j=1}^{2} \lambda_j v_j\zeta_j^2[A_jI_0(\zeta_j r) + B_jK_0(\zeta_j r)] \tag{15}$$

$$\bar{\sigma}_{rz}(r,\zeta) = -\sum_{j=1}^{2} i\lambda_j v_j\zeta\zeta_j[A_jI_1(\zeta_j r) - B_jK_1(\zeta_j r)] \tag{16}$$

where

$$\lambda_j = \frac{1+\omega_j}{v_j}, \quad j = 1,2 \tag{17}$$

and

$$\alpha = \frac{(c_{11}-c_{12})}{c_{44}}. \tag{18}$$

The eqns (11)–(16) represent the general solutions for three-dimensional axisymmetric deformations of an infinite annular elastic cylinder with finite inner and outer radii. The four arbitrary functions $A_j(\zeta)$ and $B_j(\zeta)$, $j = 1, 2$ appearing in eqns (11)–(16) can be

determined from the four traction and displacement boundary conditions associated with the inner and outer surfaces of an annular cylinder. By setting $B_1 = B_2 \equiv 0$ in eqns (11)–(16), a set of general solutions applicable for stress analysis of a solid cylinder (i.e. zero inner radius) is obtained. Some problems related to a transversely isotropic solid cylinder has been considered by Chen (1966). The general solutions applicable for stress analysis of an unbounded transversely isotropic elastic medium with a cylindrical borehole are obtained by setting $A_1 = A_2 \equiv 0$ in eqns (11)–(16). Solutions for composite cylinders can be obtained by representing the general solution of each material domain by eqns (11)–(16) and determining the arbitrary functions by considering boundary conditions at the inner and outer surfaces and continuity conditions at the material interfaces. In the remainder of this paper, attention is focused only on problems related to an unbounded transversely isotropic elastic medium with a cylindrical borehole although the methods of solution can be extended to analyse problems related to homogeneous annular/solid cylinders or composite cylinders without any fundamental difficulty.

APPLIED TRACTIONS ON BOREHOLE SURFACE

Consider a cylindrical borehole of radius a in an unbounded transversely isotropic elastic medium. A segment of the borehole surface of nondimensional length $2\hat{b}$ ($\hat{b} = b/a$) is subjected to uniformly distributed radial and tangential tractions as shown in Fig. 2. The general solutions of domain Ω are given by eqns (11)–(16) with $A_1 = A_2 \equiv 0$. The arbitrary functions B_1 and B_2 corresponding to radial traction of intensity f_0 can be determined from the following boundary conditions.

$$\sigma_{rr}(1, z) = -f_0[H(z+\hat{b}) - H(z-\hat{b})], \quad -\infty < z < \infty \tag{19}$$

$$\sigma_{rz}(1, z) = 0, \quad -\infty < z < \infty \tag{20}$$

where $H(\ldots)$ denotes the Heaviside step function.

The eqns (19) and (20) can be expressed in the Fourier transform domain as

$$\bar{\sigma}_{rr}(1, \zeta) = -\sqrt{\frac{2}{\pi}} f_0 \frac{\sin(\zeta\hat{b})}{\zeta} = \bar{f}(\zeta\hat{b}) \tag{21}$$

$$\bar{\sigma}_{rz}(1, \zeta) = 0. \tag{22}$$

Substitution of eqns (13) and (16) in eqns (21) and (22) results in the following solutions for B_1 and B_2.

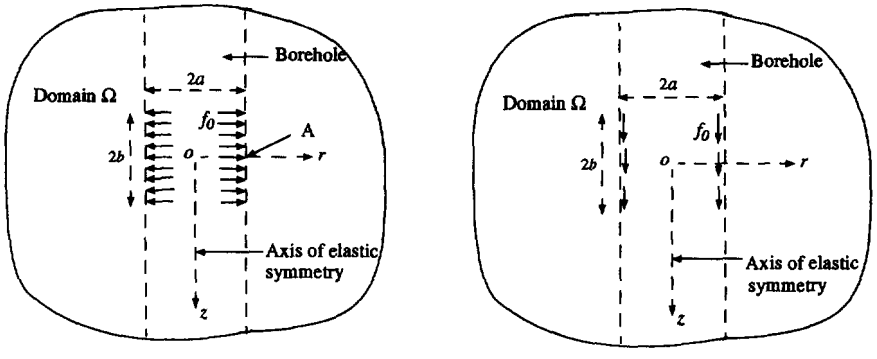

(a) Uniform radial tractions of intensity f_0 (b) Uniform tangential tractions of intensity f_0

Fig. 2. Tractions applied over a segment of borehole surface.

$$B_1(\zeta) = -\frac{\bar{f}(\zeta\hat{b})\eta_2}{[\beta_1\eta_2 - \beta_2\eta_1]} \tag{23}$$

and

$$B_2(\zeta) = -\frac{\eta_1}{\eta_2} B_1 \tag{24}$$

where

$$\beta_j = \lambda_j\zeta_j^2 K_0(\zeta_j) + \alpha\zeta_j K_1(\zeta_j), \quad j = 1, 2 \tag{25}$$

$$\eta_j = \lambda_j\nu_j\zeta_j\zeta K_1(\zeta_j), \quad j = 1, 2. \tag{26}$$

It is noted from eqns (10) and (23)–(26) that B_1 and B_2 are even functions of ζ. Therefore, it is evident from eqns (11) and (12) that the radial and vertical displacements are symmetric and antisymmetric respectively about the plane $z = 0$. The following asymptotic expressions valid for large arguments of ζ can be obtained for B_1 and B_2 by considering the asymptotic behaviour of K_n (Abramowitz and Segun, 1965)

$$B_1(\zeta) = -\frac{2}{\pi}\frac{\nu_2 f_0}{\lambda_1(\nu_1^{3/4}\nu_2 - \nu_2^{1/2}\nu_1^{5/4})}\frac{e^{\zeta_1}}{|\zeta|^{3/2}}\frac{\sin(\zeta\hat{b})}{\zeta} \tag{27}$$

$$B_2(\zeta) = \frac{2}{\pi}\frac{\nu_1 f_0}{\lambda_2(\nu_1^{1/2}\nu_2^{5/4} - \nu_2^{3/4}\nu_1)}\frac{e^{\zeta_2}}{|\zeta|^{3/2}}\frac{\sin(\zeta\hat{b})}{\zeta}. \tag{28}$$

The above asymptotic expressions are used in an ensuing section to improve the convergence of the numerical quadrature scheme used for the evaluation of semi-infinite integrals for displacements and stresses.

The arbitrary functions B_1 and B_2 corresponding to tangential tractions (Fig. 2b) applied over a segment of a borehole can be determined by considering the following boundary conditions.

$$\sigma_{rr}(1, z) = 0, \quad -\infty < z < \infty \tag{29}$$

$$\sigma_{rz}(1, z) = -f_0[H(z+\hat{b}) - H(z-\hat{b})], \quad -\infty < z < \infty. \tag{30}$$

The application of Fourier transforms to eqns (29) and (30) and the substitution of eqns (13) and (16) results in the following solutions for B_1 and B_2.

$$B_1(\zeta) = \frac{-i\bar{f}(\zeta\hat{b})\beta_2}{[\beta_1\eta_2 - \beta_2\eta_1]} \tag{31}$$

$$B_2(\zeta) = -\frac{\beta_1}{\beta_2} B_1(\zeta) \tag{32}$$

where β_j and $\eta_j (j = 1, 2)$ are defined by eqns (25) and (26) respectively.

It is noted from eqns (10), (31) and (32) that B_1 and B_2 are odd functions of ζ. Therefore, it is evident from eqns (11) and (12) that the radial and vertical displacements are antisymmetric and symmetric respectively about the plane $z = 0$. The following asymptotic expressions are obtained for B_1 and B_2.

$$B_1(\zeta) = -\frac{2}{\pi}\frac{iv_2^{3/4}f_0\sin(\zeta\hat{b})}{(v_1^{3/4}v_2^{5/4}-v_2^{3/4}v_1^{5/4})}\frac{e^{\zeta_1}}{\zeta^2|\zeta|^{1/2}} \tag{33}$$

$$B_2(\zeta) = \frac{2}{\pi}\frac{iv_1^{3/4}f_0\sin(\zeta\hat{b})}{\lambda_2(v_1^{3/4}v_2^{5/4}-v_2^{3/4}v_1^{5/4})}\frac{e^{\zeta_2}}{\zeta^2|\zeta|^{1/2}} \tag{34}$$

The arbitrary coefficients B_1 and B_2 corresponding to a radial and tangential ring load (i.e. $b \to 0$) of intensity F_0 per unit arc length can be obtained from the eqns (23), (24), (31) and (32) by setting $f_0 \sin(\zeta\hat{b})/\zeta$ as equal to $F_0/2$. The asymptotic expressions for B_1 and B_2 corresponding to radial and tangential ring loads are also obtained from eqns (27), (28), (33) and (34) by replacing the term $f_0 \sin(\zeta\hat{b})/\zeta$ by $F_0/2$.

It can be shown from the preceding analysis that the final solutions for displacements and stresses due to the loadings shown in Fig. 2 can be expressed in terms of Fourier integrals of the following type

$$I(r,z) = \int_0^\infty F(r,\zeta)\begin{Bmatrix}\sin(\zeta\hat{b})\sin(\zeta z)\\ \sin(\zeta\hat{b})\cos(\zeta z)\end{Bmatrix}d\zeta. \tag{35}$$

An examination of $F(r,\zeta)$ corresponding to displacements and stresses caused by the loadings shown in Fig. 2 indicates that it is free from any type of singularity along the path of integration for $\zeta > 0$. Furthermore it can be shown by using eqns (27), (28), (33) and (34) that $F(r,\zeta)$ behaves asymptotically in the form of $\zeta^{-n}e^{-\zeta_i(r-1)}$, $n = 1$ and 2 as $\zeta \to \infty$. A removable singularity exists in the integrand of eqn (35) at $\zeta = 0$. The application of Tauberian theorems (Wong, 1989) to the integrals corresponding to ring loads indicates that $u_r(a,z)$ due to a radial ring load and $u_z(a,z)$ due to a vertical ring load have a singularity of the form $-\ln|z|$ as $z \to 0^\pm$. On the other hand, the $u_z(a,z)$ caused by a radial ring load and $u_r(a,z)$ caused by a vertical ring load possess a finite discontinuity at $z = 0^\pm$. The above behaviour of displacements is similar to that observed in the classical Flamant solution (Timoshenko and Goodier, 1970) for an elastic half plane subjected to concentrated loads at the surface. Parnes (1984) also observed a logarithmic singularity in the $u_r(a,0)$ due to a radial ring load applied to a borehole in an isotropic medium. The solutions for ring loadings derived here are useful in the analysis of a variety of problems related to geomechanics and composite materials. In the ensuing section some applications of the above solutions are considered.

RIGID INCLUSION IN A BOREHOLE

In this section, contact problems involving a rigid cylinder bonded to a borehole in an infinite transversely isotropic elastic medium are considered. The Fig. 3(a) shows an axially loaded rigid cylinder of radius a and height h bonded to a borehole. The quantities of interest are the vertical displacement Δ_z of the cylinder and stresses along the contact surface caused by the load P_0. Problems of this nature are useful in the theoretical idealization of response of borehole plugs and anchors, fiber pull-out tests, study of load diffusion and interface behaviour of broken/debonded fibres and the matrix material, etc. Although it is assumed here that the cylinder is rigid, the case of a flexible cylinder under an axial load could be analysed by coupling the solutions for a ring load derived in the preceding section with one-dimensional governing equation for axial deformation of an elastic bar.

The Fig. 3(b) shows another type of contact problem where a rigid cylinder with a radial misfit of Δ_r is placed in a borehole. Analyses of problems of this nature are useful in the development of in situ testing devices such as a pressuremeter for measurement of anisotropy of geological materials. It is usually assumed that the pressure exerted by a pressuremeter is uniform and the solutions derived in the preceding section can be used in the analysis. However, it is useful to examine the solutions corresponding to uniform radial displacement of the borehole with that corresponding to uniform radial pressure. The

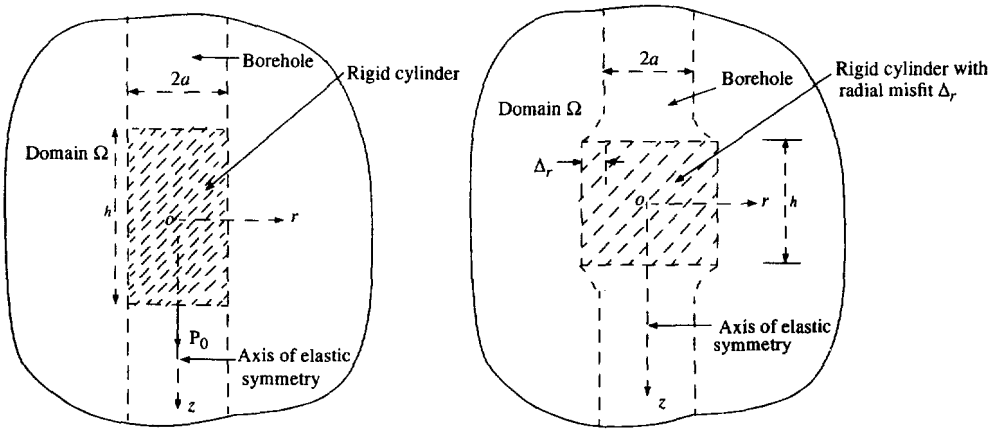

Fig. 3. Contact problems involving a rigid cylinder and a borehole.

system shown in Fig. 3(b) is also useful in the study of interfacial stresses due to a radial misfit between a fibre and a matrix material. Such a misfit exists in composites during high temperature processing due to differences in magnitude of the thermal expansion coefficient of fibres and matrix materials. High compressive residual stresses exist in a fiber-matrix interface whenever the thermal expansion coefficient of a matrix is greater than that of a fiber. The interfacial normal stress mobilizes the frictional resistance along a fiber-matrix interface during loading.

The problems shown in Fig. 3 can be formulated in terms of a pair of coupled singular integral equations. Let $\tau_j(z')$, $j = r, z$ denote the traction at a point $(1, z')$ on the contact surface. Then the displacement $u_i(r, z)$, $i = r, z$ at an arbitrary point in the domain Ω can be expressed as

$$\int_{-\hat{h}/2}^{\hat{h}/2} G_{ij}(r, z; 1, z')\tau_j(z')\,dz' = u_i(r, z), \quad i, j = r, z; |z| \leqslant \hat{h}/2 \tag{36}$$

where $\hat{h} = h/a$ and the Green's function $G_{ij}(r, z; 1, z')$ denotes the displacement in the i-direction at point (r, z) in the domain Ω caused by a ring load of unit intensity (per arc length) in the j-direction applied through the point $(1, z')$ on the contact surface. Note that summation is implied on the index j in eqn (36). Explicit analytical solutions for the Green's function G_{ij} are given in the preceding section. The displacement u_i on the contact surface can be expressed as

$$u_z(1, z) = \Delta_z, \quad |z| \leqslant \hat{h}/2 \tag{37a}$$

$$u_r(1, z) = 0, \quad |z| \leqslant \hat{h}/2 \tag{37b}$$

for the axial loading problem shown in Fig. 3a and

$$u_z(1, z) = 0, \quad |z| \leqslant \hat{h}/2 \tag{38a}$$

$$u_r(1, z) = \Delta_r, \quad |z| \leqslant \hat{h}/2 \tag{38b}$$

for the problem shown in Fig. 3b.

The resultant axial force P_0 corresponding to the system shown in Fig. 3(a) can be expressed as

$$P_0 = 2\pi c_{44} a^2 \int_{-\hat{h}/2}^{\hat{h}/2} \tau_z(z)\,\mathrm{d}z. \tag{39}$$

The average radial stress q_0 corresponding to the system shown in Fig. 3(b) can be expressed as

$$q_0 = \frac{c_{44}}{\hat{h}} \int_{-\hat{h}/2}^{\hat{h}/2} \tau_r(z)\,\mathrm{d}z. \tag{40}$$

The coupled singular integral equation system given by eqn (36) can be solved only by numerical techniques due to the complexity of the kernel function G_{ij}. Noting that G_{ij} is integrable with respect to z', the eqn (36) is replaced by the following linear simultaneous equation system which is obtained by discretizing the contact region $|z| \leqslant \hat{h}/2$ by N node points and assuming that the tractions $\tau_j(z_n)$ corresponding to the nth node point are uniformly distributed over its tributary length.

$$\sum_{n=1}^{N} G_{ij}^{*}(1, z_m; 1, z_n)\tau_j(z_n) = u_i(1, z_m), \quad m = 1, 2, \ldots, N; i, j = r, z \tag{41}$$

where the influence function G_{ij}^{*} denote the displacement in the i-direction at the mth node point with coordinates $(1, z_m)$ due to uniform traction of unit intensity in the j-direction applied over the tributary length of the nth node point with coordinates $(1, z_n)$. Explicit analytical solutions for G_{ij}^{*} are given in the preceding section and G_{ij}^{*} is a non-singular influence function. The eqn (41) can be solved directly for nodal contact tractions by setting $\Delta_z = 1$ in eqn (37) or $\Delta_r = 1$ in eqn (38). Thereafter, eqns (39) and (40) can be used to compute the axial stiffness and average radial stress respectively. A singularity exists in the contact stress field at the two edges of the inclusion ($z = -h/2$ and $z = h/2$) in the present class of problems (Williams, 1952; Luk and Keer, 1979). The accuracy of contact stresses obtained from the numerical solution of eqn (41) can be improved by taking more node points near the two edges. However, care should be taken not to define nodal points very close to each other ($<0.05a$) since the coefficient matrix of eqn (41) may become ill-conditioned due to the presence of a logarithmic singularity in G_{ij}^{*} as the nodal tributary length approaches zero. The order of singularities in the traction field can be determined by considering a two dimensional analysis (Williams, 1952). It can be shown that the singularities in the traction field are of the classical square-root type since the wedge angle corresponding to the present case is equal to π.

NUMERICAL RESULTS AND DISCUSSION

Numerical scheme

The computation of elastic fields corresponding to the problems shown in Figs 2 and 3 involves the numerical evaluation of semi-infinite integrals of the form given by eqn (35). These integrals cannot be evaluated analytically due to the complex nature of the integrands. However, these types of integrals can be accurately computed by using a variety of numerical quadrature schemes. In the present study, the authors use the trapezoidal rule with the integration interval, $\Delta\zeta = 0.1$. The application of direct numerical quadrature to the integrals given by eqn (35) can be quite inefficient since the integrands decay as $\zeta^{-n}(n = 1, 2)$ when $r/a = 1$ (i.e., at the borehole surface). For $r/a > 1$, the integrand decays exponentially in the form $\zeta^{-n}e^{-\zeta_i(r-1)}$. The accuracy and the convergence of the numerical integration scheme can be improved by expressing eqn (35) in the following form [except for one special case of $F(\zeta, r)$ which requires an additional modification].

$$I = \int_0^\infty [F(\zeta, r) - F^*(\zeta, r)] \begin{Bmatrix} \sin(\zeta\hat{b}) \sin(\zeta z) \\ \sin(\zeta\hat{b}) \cos(\zeta z) \end{Bmatrix} d\zeta + I_0 \tag{42}$$

where

$$I_0 = \int_0^\infty F^*(\zeta, r) \begin{Bmatrix} \sin(\zeta\hat{b}) \sin(\zeta z) \\ \sin(\zeta\hat{b}) \cos(\zeta z) \end{Bmatrix} d\zeta \tag{43}$$

$$F^*(\zeta, r) = C \frac{e^{-\zeta_1(r-1)}}{\zeta^n}, \quad n = 1, 2. \tag{44}$$

$F^*(\zeta, r)$ is the asymptotic form of $F(\zeta, r)$, and C is a constant. An explicit representation for F^* is obtained by substituting eqns (27), (28), (33) and (34) and the asymptotic expressions for modified Bessel functions (Abramowitz and Segun, 1965) in the final solutions. Because of similar asymptotic behaviour of F and F^*, the semi-infinite integral in eqn (42) decays rapidly and can be truncated at a relatively small value of ζ as the upper limit of the integral. The integral I_0 has the following closed form solutions (Gradshteyn and Ryzhik, 1980) for different forms of F^*.

$$\int_0^\infty \zeta^{-1} e^{-\beta\zeta} \sin\zeta\hat{b} \sin\zeta z \, d\zeta = \tfrac{1}{4} \ln \left[\frac{\beta^2 + (\hat{b}+z)^2}{\beta^2 + (\hat{b}-z)^2} \right], \tag{45}$$

$$\int_0^\infty \zeta^{-2} e^{-\beta\zeta} \sin\zeta\hat{b} \sin\zeta z \, d\zeta = \frac{\hat{b}}{2} \tan^{-1} \left(\frac{2\beta z}{\beta^2 + \hat{b}^2 - z^2} \right) + \frac{z}{2} \tan^{-1} \left(\frac{2\beta\hat{b}}{\beta^2 + z^2 - \hat{b}^2} \right) + \frac{\beta}{4} \ln \left[\frac{\beta^2 + (\hat{b}-z)^2}{\beta^2 + (\hat{b}+z)^2} \right], \tag{46}$$

$$\int_0^\infty \zeta^{-1} e^{-\beta\zeta} \sin\zeta\hat{b} \cos\zeta z \, d\zeta = \tfrac{1}{2} \tan^{-1} \left(\frac{2\beta\hat{b}}{\beta^2 - \hat{b}^2 + z^2} \right) + \gamma \frac{\pi}{2},$$

$$\gamma = 0 \quad \text{for} \quad \beta^2 - \hat{b}^2 + z^2 \geqslant 0,$$

$$\gamma = 1 \quad \text{for} \quad \beta^2 - \hat{b}^2 + z^2 < 0. \tag{47}$$

The computation of integrals of the form $\int_0^\infty F(\zeta, r) \sin(\zeta\hat{b}) \cos(\zeta z) \, d\zeta$ when $F(\zeta, r)$ is equal to $\zeta^{-2} e^{-\beta\zeta}$ requires a modification of eqn (42) since a closed form solution for the corresponding I_0 does not exist if the lower limit of the integrand is equal to zero. To compute the relevant integrals let

$$I_1 = \int_0^1 F(\zeta, r) \sin(\zeta\hat{b}) \cos(\zeta z) \, d\zeta + \int_1^\infty [F(\zeta, r) - F^*(\zeta, r)] \sin(\zeta\hat{b}) \cos(\zeta z) \, d\zeta + I^* \tag{48}$$

where

$$I^* = C \int_1^\infty \zeta^{-2} e^{-\beta\zeta} \sin(\zeta\hat{b}) \cos(\zeta z) \, d\zeta. \tag{49}$$

The integrand of the second integral of eqn (48) decays rapidly due to similar asymptotic

Table 1. Comparison of solutions along the borehole surface ($r/a = 1$) due to a radial ring load (Poisson's ratio = 0.25)

z/a	$c_{44}u_r(a,z)/F_0$		$c_{44}u_z(a,z)/F_0$	
	Present study	Parnes (1983a)	Present study	Parnes (1983a)
0.25	0.255	0.26	−0.097	−0.09
0.50	0.132	0.13	−0.076	−0.07
1.0	0.055	0.06	−0.051	−0.05
1.5	0.027	0.03	−0.035	−0.04

Table 2. Comparison of solutions along the plane $z = 0$ due to radial ring loading applied to borehole surface (Poisson's ratio = 0.25)

r/a	$c_{44}u_r(r,0)/F_0$		$a\sigma_{rr}(r,0)/F_0$		$a\sigma_{\theta\theta}(r,0)/F_0$	
	Present study	Parnes (1983a)	Present study	Parnes (1983a)	Present study	Parnes (1983a)
1.25	0.355	0.35	−2.08	—	0.255	0.23
1.50	0.216	0.21	−0.832	−0.83	0.171	0.17
2.0	0.111	0.11	−0.276	−0.27	0.077	0.08
2.5	0.069	0.07	−0.130	−0.14	0.040	0.04
3.0	0.047	0.04	−0.072	−0.07	0.023	0.02

behavior of F and F^*. The integral I^* defined by eqn (49) could be evaluated by the following procedure.

$$\int_1^\infty \zeta^{-2}e^{-\beta\zeta}\sin(\zeta\hat{b})\cos(\zeta z)\,d\zeta = \frac{1}{2}\int_1^\infty \zeta^{-2}e^{-\beta\zeta}[\sin(\hat{b}-z)\zeta+\sin(\hat{b}+z)\zeta]\,d\zeta \tag{50}$$

$$\int_1^\infty \zeta^{-2}e^{-\beta\zeta}\sin(p\zeta)\,d\zeta = \{e^{-\beta}\sin p-\beta\,\mathrm{Im}[E_1(\beta+ip)]-p\,\mathrm{Re}[E_1(\beta+ip)]\} \tag{51}$$

where $E_1(\ldots)$ is the exponential integral which can be evaluated by using a series expansion (Abramowitz and Stegun, 1965).

The exponential term in $F^*(\zeta, r)$ in eqn (44) vanishes at $r = 1$ (i.e., at the borehole surface). A different set of closed form expressions can be obtained from Gradshteyn and Ryzhik (1980) for the integrals appearing in eqns (45) and (47) when $\beta = 0$. The closed form solution for I^* corresponding to eqn (48) when $\beta = 0$ can be expressed in terms of sine and cosine integrals (Abramowitz and Stegun, 1965).

Tables 1 and 2 present comparisons of numerical solutions for displacements and stresses with those presented by Parnes (1983a) for an isotropic medium (Poisson's ratio = 0.25) with a cylindrical borehole subjected to a radial ring load of intensity F_0. The agreement between present solutions and those reported by Parnes (1983a) is very good. Results due to Parnes (1983a) are directly taken from figures in his paper and can be measured only with two decimal accuracy. It is also found that the direct numerical integration of Fourier integrals without using eqns (42) results in solutions that are very close to the solutions reported in Tables 1 and 2. However in this case the value of the upper limit of the semi-infinite integrals required for convergence of numerical solutions is found to be very large (e.g. $\zeta > 100$).

Displacements and stresses caused by applied tractions

Fig. 4a shows the nondimensional radial displacement $[(c_{44}u_r(a,0))/(f_0a)]$ due to radial tractions of uniform intensity f_0 applied to the borehole surface. Solutions are presented for $\hat{b} = b/a$ varying from 0.1 to 5.0 and for the four different types of materials whose properties are defined in Table 3 (Payton, 1983; Wang, 1992). A nondimensional material constant $\hat{c}_{ij} = c_{ij}/c_{44}$ is used in Table 3. The radial displacement at the centre of a loading

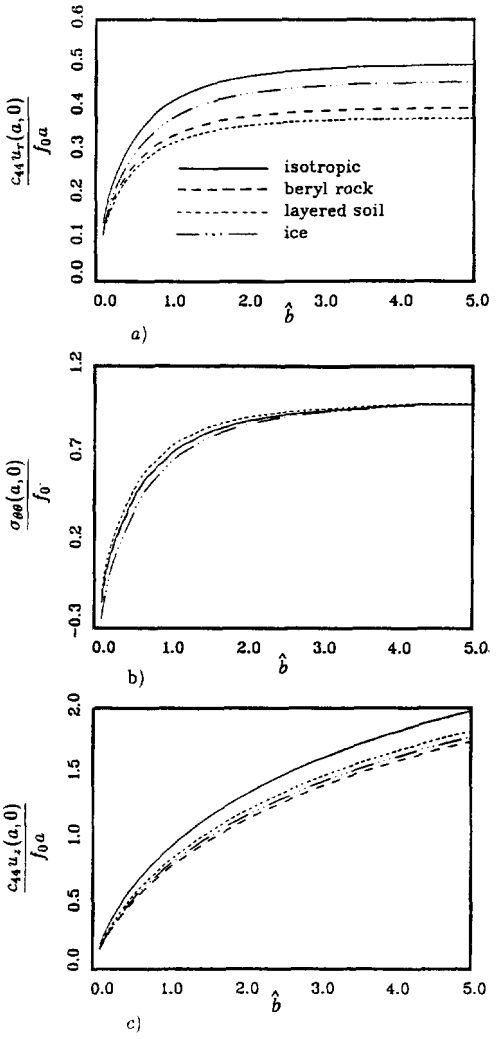

Fig. 4. Variation of (a) central radial displacement and (b) central hoop stress caused by radial traction, and (c) central vertical displacement caused by tangential traction with respect to $\hat{b}$.

Table 3. Material constants

	c_{11}/c_{44}	c_{12}/c_{44}	c_{33}/c_{44}	c_{13}/c_{44}
Isotropic	3.00	1.00	3.00	0.99
Layered soil	4.13	1.47	3.60	1.01
Beryl rock	3.90	1.40	5.10	1.80
Ice	4.21	2.03	4.53	1.62
Glass-epoxy composite	3.17	1.40	10.0	1.10
Graphite-epoxy composite	2.02	0.68	21.2	0.07

segment has a singularity of the form $-\ln|z|$ when $\hat{b} = 0$. The singular behaviour is also evident from the numerical solutions presented in Fig. 4a. At the limit, $\hat{b} \to \infty$, the radial traction problem is identical to the Lame problem in classical elasticity (Timoshenko and Goodier, 1970) and the radial displacement should approach the corresponding plane strain limit of $1/(\hat{c}_{11} - \hat{c}_{12})$, which is found to be independent of Poisson's ratio ν for an isotropic material since $\hat{c}_{11} = 2(1-\nu)/(1-2\nu)$ and $\hat{c}_{12} = 2\nu/(1-2\nu)$. Since the plane strain solution is inversely proportional to $(\hat{c}_{11} - \hat{c}_{12})$, it is noted from Table 3 that the isotropic material has the largest nondimensional radial displacement followed by ice, beryl rock and layered soil. Solutions presented in Fig. 4a also confirm that the above order of magnitude of radial displacement is valid for other values of $\hat{b}$ as well. The plane strain solution is approached

when $\hat{b} > 3.0$. The influence of material anisotropy on radial displacement is noted for all values of $\hat{b}$ except for $\hat{b} < 0.2$.

Figure 4b shows the solutions for nondimensional hoop stress $[\sigma_{\theta\theta}(a,0)/f_0]$ caused by uniform radial tractions (Fig. 2a). For very small values of $\hat{b}$ (e.g. $\hat{b} < 0.2$), hoop stress is compressive for the four different materials. The existence of a compressive hoop stress under a radial ring load ($\hat{b} = 0$) was observed by Parnes (1983) for isotropic materials with Poisson's ratio greater than zero. The order of singularity of $\sigma_{\theta\theta}(a,z)$ corresponding to a ring load is $-\ln|z|$ as $|z| \to 0$. The influence of material anisotropy on hoop stress is relatively small. The nondimensional hoop stress corresponding to the plane strain case is 1.0 for all transversely isotropic materials. The hoop stress solutions for isotropic material and beryl rock are almost identical. The hoop stresses for ice and layered soil are slightly smaller and larger than the solutions for isotropic materials respectively for $\hat{b} < 3.0$.

The Fig. 4c shows the solutions for nondimensional vertical displacement $[c_{44}u_z(a,0)/f_0 a]$ at the centre of a loading segment due to uniform tangential traction of intensity f_0 (Fig. 2b). It can be shown that for a ring load (i.e. $b = 0$), $u_z(a,z) \to -\ln|z|$ as $|z| \to 0$, similar to the case of $u_r(a,z)$ due to a radial ring load. Note that $u_z(r,z)$ corresponding to tangential tractions at the limit $\hat{b} \to \infty$ is singular. The case corresponding to $\hat{b} \to \infty$ represents a anti-plane problem. For example, the vertical displacement for the anti-plane case is given by

$$u_z(r) = \frac{f_0}{c_{44}} \int_1^{r_0} \frac{\mathrm{d}r}{r} \tag{52}$$

where r_0 is the outer radius of the medium. Since $r_0 \to \infty$ in the present case (infinite medium), the vertical displacement corresponding to the anti-plane case is singular. For the finite values of $\hat{b}$ considered in the numerical study ($0.1 \leqslant \hat{b} \leqslant 5.0$), it is found that the isotropic material undergoes the largest vertical displacement followed by layered soil, ice and beryl rock. The nondimensional vertical displacement is found to be inversely proportional to $\hat{c}_{33}$ in Table 3. It can be intuitively suggested that $\hat{c}_{33}$ representing the stiffness in the vertical direction has the most significant influence on u_z for a finite value of $\hat{b}$. At the anti-plane limit, u_z is infinite and independent of $\hat{c}_{33}$.

Figures 5 and 6 show the radial displacement, radial stress, hoop stress and vertical stress along the plane $z/a = 0$ caused by uniform radial tractions with $\hat{b} = 0.5$ and 1.5, respectively. The radial displacement corresponding to the four materials decays rapidly with the radial distance. The decay of radial displacement is steeper for low values of $\hat{b}$ and becomes equal to the plane strain decay of $1/r$ for $\hat{b} > 3.0$. The influence of material anisotropy on $u_r(r,0)$ is similar to that observed in Fig. 4a. Comparison of solutions for nondimensional radial stress $[\sigma_{rr}(r,0)/f_0]$ in Figs 5 and 6 indicates that σ_{rr} decreases more rapidly with the radial distance when compared to $u_r(r,0)$. For $\hat{b} = 0.5$ and 1.5 the radial stress at $r/a = 3.0$ is less than fifteen percent of the applied stress at $r = a$. Numerical solutions indicate that for $\hat{b} > 3.0$, the variation of $\sigma_{rr}(r,0)$ with r is very close to the r^{-2} type variation corresponding to the plane strain case. The material anisotropy has a negligible influence on radial stress.

The solutions for nondimensional hoop stress $[\sigma_{\theta\theta}(r,0)/f_0]$ in Figs 5 and 6 show a behaviour which is similar to the radial stress profiles although $\sigma_{\theta\theta}(r,0)$ decreases more rapidly with the radial distance when compared to $\sigma_{rr}(r,0)$. A minor influence of anisotropy is noted in the hoop stress solutions in the domain $1.0 \leqslant r/a \leqslant 3.0$ for $\hat{b} \geqslant 1.0$. The hoop stress at all interior points becomes proportional to the plane strain value of r^{-2} for $\hat{b} > 3.0$. The vertical stress $[\sigma_{zz}(a,0)/f_0]$ is compressive along the plane $z/a = 0$ and the peak values are observed at the borehole surface ($r = a$). The vertical stress decays very rapidly with the radial distance and is negligible for $r/a > 3.0$. The magnitude of compressive vertical stress decreases at points within the medium with increasing $\hat{b}$. The influence of material anisotropy is noted in the vertical stress only near the borehole surface ($1 \leqslant r/a \leqslant 2$) for $\hat{b} > 1.0$. The solution for σ_{zz} at the plane strain limit ($\hat{b} \to \infty$) also become equal to zero.

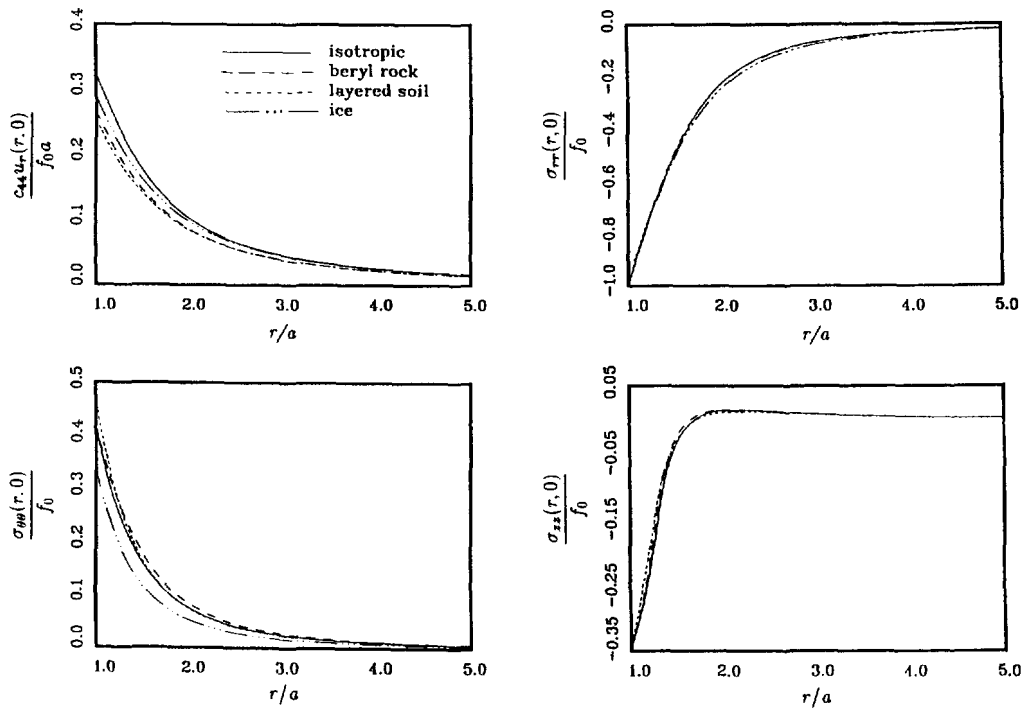

Fig. 5. Radial variation of elastic fields caused by uniform radial traction ($\hat{b} = 0.5$).

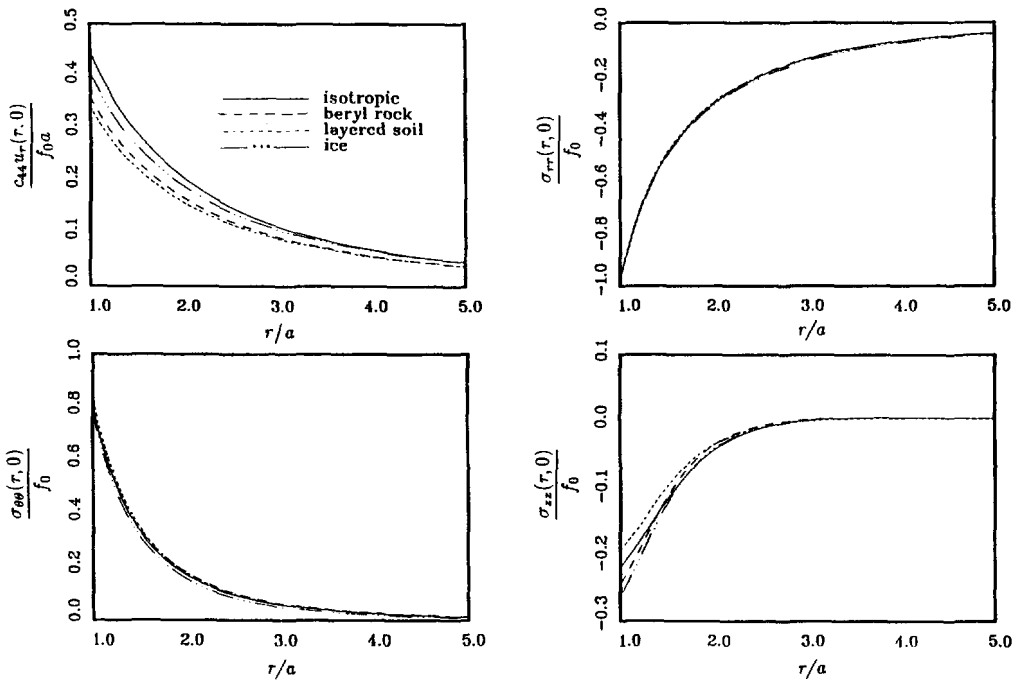

Fig. 6. Radial variation of elastic fields caused by uniform radial traction ($\hat{b} = 1.5$).

Note that $u_z(r,0)$ and $\sigma_{rz}(r,0)$ due to radial tractions are zero since these quantities are antisymmetric with respect to the plane $z = 0$.

Figure 7 shows the nondimensional vertical displacement $[c_{44}u_z(r,0)/af_0]$ and shear stress $[\sigma_{rz}(r,0)/f_0]$ along the plane $z = 0$ due to a uniform tangential traction of intensity f_0 (Fig. 2b) with $\hat{b} = 0.5$ and 1.5. It is noted that $u_z(r,0)$ decays rapidly with the radial distance. The vertical displacement at interior points increases with increasing $\hat{b}$. The anti-plane solution yields singular vertical displacements as shown previously. The influence of material anisotropy on $u_z(r,0)$ is noted at all interior points. The shear stress $\sigma_{rz}(r,0)$

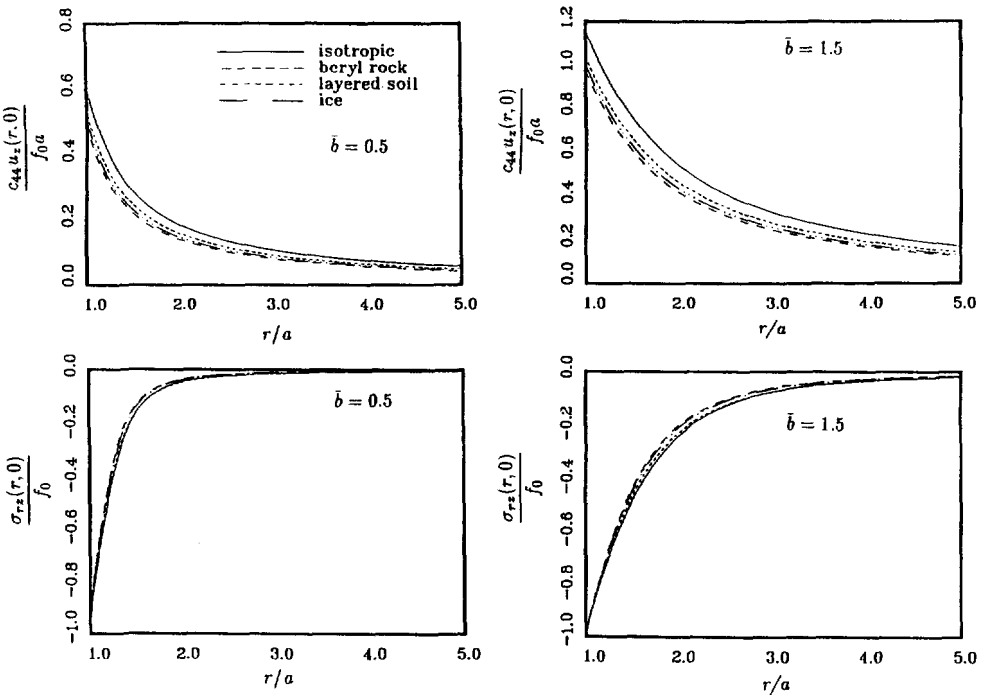

Fig. 7. Radial variation of vertical displacement and shear stress caused by uniform tangential traction.

decreases more rapidly with the radial distance when compared to the vertical displacement. For the anti-plane case ($\hat{b} \to \infty$), the variation of σ_{rz} with r is equal to r^{-1}. The influence of material anisotropy on shear stress is negligible. It is noted that u_r, σ_{rr}, $\sigma_{\theta\theta}$ and σ_{zz} due to uniform tangential tractions are zero along the plane $z/a = 0.0$.

Numerical solutions for contact problems

In this section, numerical solutions corresponding to contact problems shown in Fig. 3 are presented for different length-radius ratios of the inclusion and for the five different materials whose properties are defined in Table 3. Figure 8a shows nondimensional average value of radial stress ($q_0 a/c_{44}\Delta_r$) as defined by eqn (40) for an inclusion with a radial misfit of Δ_r and $0.5 \leqslant h/a \leqslant 10.0$. It is noted that very large compressive radial stresses can be developed at the interface for small values of h/a. The magnitude of interfacial radial stress depends significantly on the aspect ratio of an inclusion (i.e. h/a) and the degree of material anisotropy. A plane strain condition is reached when $h/a > 10$. It can be shown that in the plane strain case, $q_0 a/c_{44}\Delta_r = -(\hat{c}_{11} - \hat{c}_{12})$. Table 3 and Fig. 8a show that the largest compressive stress under the plane strain condition is associated with layered soil followed by beryl rock, isotropic material, glass-expoxy and graphite-epoxy. This order of magnitude of radial stress is found to be valid for other values of h/a as well. The problem shown in Fig. 3b was also analysed under the condition that τ_z in eqn (41) is zero along the contact surface (i.e. smooth contact). The numerical solutions for q_0 under smooth contact condition differ less than five percent from that corresponding to the fully bonded case.

Figure 8b shows the maximum tensile hoop stress $[\sigma_{\theta\theta}^{max} a/c_{44}\Delta_r]$ at the contact surface for an inclusion with a radial mis-fit of Δ_r. The maximum tensile hoop stress occurs at $z/a = 0$. An examination of the hoop stress profile along the contact surface indicates that it is compressive and singular at the two edges (i.e. $z = -h/2$ and $h/2$). The solutions for maximum tensile hoop stress approach the corresponding plane strain value of $(\hat{c}_{11} - \hat{c}_{12})$ for $h/a > 3.0$. The order of magnitude of hoop stress solutions shown in Fig. 8b is similar to that of the average radial stress shown in Fig. 8a. Since the largest tensile hoop stress exists under the plane strain case, it can be concluded that the possibility of tensile cracking around an inclusion is much higher if $h/a > 3.0$.

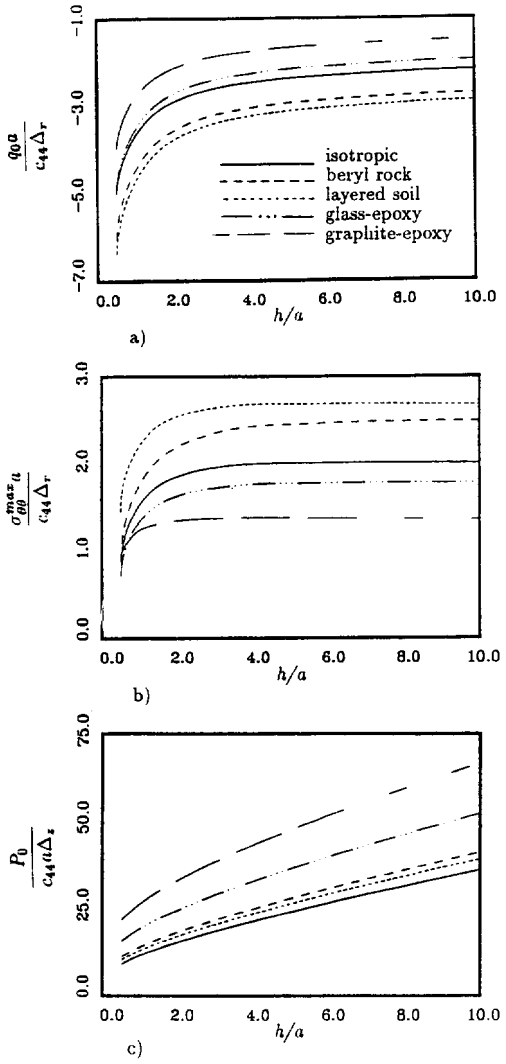

Fig. 8. Variation of (a) average radial traction and (b) maximum tensile hoop stress due to radial misfit Δ_r, and (c) axial stiffness of a rigid cylinder with length-radius ratio.

Figure 8c shows the axial stiffness $[P_0/c_{44}a\Delta_z]$ of a rigid cylinder bonded to a borehole surface (Fig. 3a). Solutions are presented for $0.25 < h/a < 10.0$. The influence of material anisotropy is clearly evident in these solutions especially for the two composite materials. The order of magnitude of axial stiffness for different materials is similar to that of $\hat{c}_{33}$ in Table 3. Similar behaviour was observed earlier for the vertical displacement under tangential tractions. The variation of axial stiffness with the aspect ratio h/a is almost linear for $h/a > 3.0$. For the anti-plane problem ($h/a \to \infty$), the axial stiffness is infinite. The problem shown in Fig. 3a was also analysed under the condition that the traction τ_r is equal to zero along the contact surface and the solutions for axial stiffness was found to be very close to the solutions shown in Fig. 8c.

It is useful to compare the stiffness of a rigid cylinder bonded to a borehole with that of a partially embedded rigid cylinder in an elastic half space (Luk and Keer, 1979; Selvadurai and Rajapakse, 1985) and investigate the applicability of the borehole model to approximate half space problems. Table 4 presents a comparison of axial stiffness of a rigid cylinder of radius a and height h bonded to a borehole in an infinite isotropic medium with that of a rigid cylinder of radius a and height $2h$ partially embedded in an isotropic elastic half space. The number of nodes (N) used to discretize the contact surface is also given in Table 4. The difference between the two sets of solutions in Table 4 is less than five percent for $h/a > 0.25$. This relationship between the two sets of solutions indicates, for example,

Table 4. Comparison of axial stiffness of a rigid cylinder/shell of length h in a borehole and a rigid cylinder of length $2h$ in an elastic half space (Poisson's ratio = 0.3)

		$P_0/c_{44}a\Delta_z$	
h/a	N	Cylinder-borehole model	Cylinder-half space model for $2h/a$
0.25	10	7.73	7.45*
0.50	20	9.47	8.85*
1.0	30	11.97	11.34*
2.5	40	17.92	17.71*
5.0	50	24.22	24.1†
10.0	50	37.35	36.9†

* Luk and Keer (1979).
† Selvadurai and Rajapakse (1985), Poisson's ratio = 0.25.

the global quantities such as pull-out forces and axial stiffness of piles and anchors can be evaluated by using a borehole model instead of using a half space model.

The radial stress $[\sigma_{rr}(a,z)a/c_{44}\Delta_r]$ and hoop stress $[\sigma_{\theta\theta}(a,z)a/c_{44}\Delta_r]$ along the contact surface of rigid cylinders ($h/a = 1.0, 2.0$) with a radial mis-fit are shown in Fig. 9. A significant dependence of radial stress on the material anisotropy is noted. The radial contact stress is symmetric about the $z = 0$ plane and compressive throughout the contact surface. The radial stress at the two edges ($z = -h/2$ and $h/2$) is singular (square root type) and it is nearly constant over the central part of the contact surface. As h/a increases, the radial stress in the central part of an inclusion decreases and approaches the plane strain value of $-(\hat{c}_{11}-\hat{c}_{12})$. The hoop stress profiles shown in Fig. 9 are similar to the radial stress profiles except that the hoop stress in the central part of an inclusion is tensile while it is compressive and singular near the edges. The order of magnitude of tensile hoop stresses for different materials is similar to that of compressive radial stresses. The tensile hoop stress in a central part of an inclusion increases with h/a and approaches the plane strain value of $(\hat{c}_{11}-\hat{c}_{12})$ for $h/a > 3.0$.

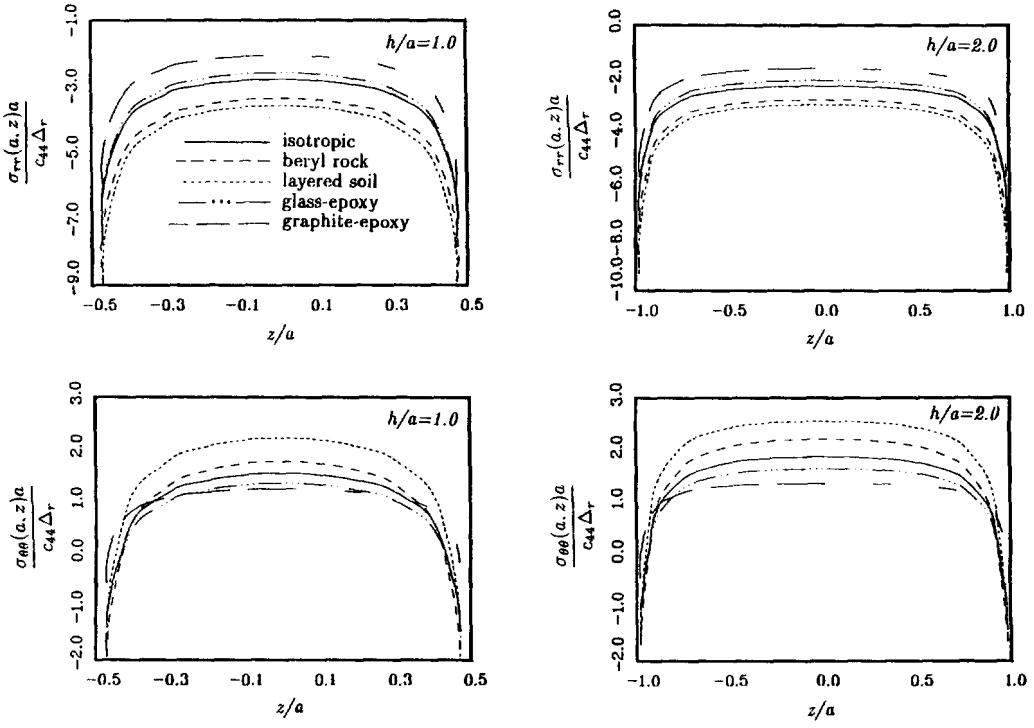

Fig. 9. Variation of radial and hoop stresses along the contract surface of a rigid cylinder with a radial misfit of Δ_r.

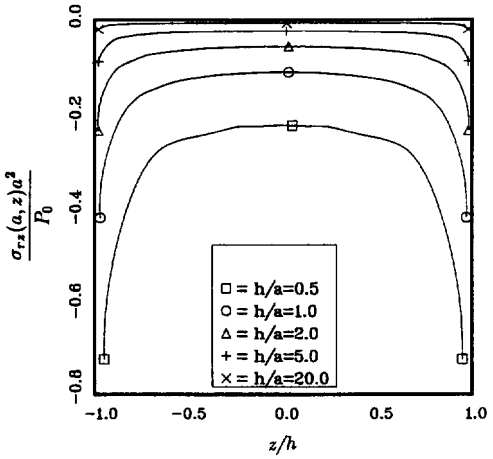

Fig. 10. Profiles of σ_{rz} along the contact surface of an axially loaded rigid cylinder bonded to a borehole in an isotropic medium (Poisson's ratio = 0.25).

Figure 10 shows the nondimensional shear stress $[\sigma_{rz}(a,z)a^2/P_0]$ along the contact surface of an axially loaded rigid cylinder bonded to a borehole in an isotropic medium. The shear stress σ_{rz} is symmetric about the $z = 0$ plane and has a square-root type singularity at the two edges. It is nearly constant over the central part of contact surface and decreases with increasing h/a. The influence of material anisotropy is found to be negligible on σ_{rz}. Therefore the solutions are presented only for an isotropic material. The contact stress σ_{rr} is antisymmetric about $z = 0$ and singular along the edges of a cylinder, and is not shown here for brevity.

CONCLUSIONS

The Fourier transforms of general solution for axisymmetric displacements and stresses of a transversely isotropic annular cylinder of infinite length are derived in terms of modified Bessel functions. These general solutions are used to solve boundary-value problems involving a borehole subjected to normal and tangential tractions, and a rigid cylinder bonded to a borehole. An efficient numerical integration scheme based on the asymptotic behaviour of the integrands is used to compute the Fourier integrals encountered in the present analysis. The accuracy of present solutions is confirmed by comparison with the solutions given by Parnes (1983a).

It is found that material anisotropy has a significant influence on displacements caused by tractions applied to a borehole surface but a negligible influence on stresses. The order of magnitude of nondimensional radial displacement due to uniform radial traction is proportional to $(\hat{c}_{11}-\hat{c}_{12})^{-1}$. Plane strain conditions are reached when $\hat{b} > 3.0$ and the elastic fields depend significantly on $\hat{b}$ when $\hat{b} < 3.0$. Elastic fields caused by applied tractions are negligible for $r/a > 4.0$ if $\hat{b} < 2.0$. Therefore the response of a thick annular cylinder can be approximated by that of a borehole in an infinite medium under certain conditions. Hoop stress at the centre of a radial loading segment with $\hat{b} < 0.2$ is compressive for all materials considered in the present study. Peak stresses are noted at $r = a$ for both radial and tangential tractions.

The average radial contact stress and maximum tensile hoop stress of a rigid cylinder with a radial misfit depend significantly on the material anisotropy and aspect ratio. Plane strain conditions are reached when $h/a > 10.0$ for a rigid cylinder with a radial misfit. The order of magnitude of average radial stress and the maximum tensile hoop stress is proportional to $(\hat{c}_{11}-\hat{c}_{12})$. Radial and hoop stresses are singular and compressive at the edges of a cylinder. Axial stiffness of a rigid cylinder bonded to a borehole increases with h/a. The influence of material anisotropy on axial stiffness is governed mainly by the material constant $\hat{c}_{33}$. The axial stiffness of a rigid cylinder with aspect ratio h/a bonded to a borehole is nearly equal to that of a rigid cylinder with aspect ratio $2h/a$ partially

embedded in an elastic half space. Therefore the borehole model can be used to compute the axial stiffness of cylindrical piles and anchors, and pull-out forces.

Acknowledgements—The first author is grateful to the Alexander von Humboldt Foundation of Germany for awarding a research fellowship. TH Darmstadt and the University of Manitoba provided research facilities and granted leave to the first author respectively. Ulrich Hueck, Stefan Heimer and Yafei Zhou assisted in the preparation of figures.

REFERENCES

Abramowitz, M. and Stegun, I. A. (1965). *Handbook of Mathematical Functions*, Dover Publications, New York.
Chen, W. T. (1966). On some problems in transversely isotropic materials. *J. Appl. Mech.* **33,** 347–355.
Eubanks, R. A. and Sternberg, E. (1954). On the axisymmetric problem of elasticity theory for a medium with transverse isotropy. *J. Rat. Mech. Anal.* **3,** 89–98.
Gibson, R. E. (1972). The analytical method in soil mechanics. *Geotechnique* **24,** 115–140.
Gradshteyn, I. S. and Ryzhik, I. M. (1980). *Table of Integrals, Series and Products*, Academic Press, New York.
Green, A. E. and Zerna, W. (1968). *Theoretical Elasticity*, Clarendon Press, Oxford, U.K.
Jordan, D. W. (1962). The stress waves from a finite cylindrical explosive source. *J. Math. Mech.* **11,** 503–551.
Lekhnitskii, S. G. (1963). *Theory of Anisotropic Elastic Bodies*, Holden-Day, San Francisco, CA.
Luk, V. K. and Keer, L. M. (1979). Stress analysis for an elastic half-space containing an axially-loaded rigid cylindrical rod. *Int. J. Solids Structures* **15,** 805–827.
Muki, R. and Sterberg, E. (1969). On the diffusion of an axial load from an infinite cylindrical bar embedded in an elastic medium. *Int. J. Solids Structures* **5,** 587–605.
Parnes, R. (1983a). Applied tractions on the surface of an infinite cylindrical bore. *Int. J. Solids Structures* **19,** 165–177.
Parnes, R. (1983b). Elastic response to a time-harmonic torsion-force acting on a bore surface. *Int. J. Solids Structures* **19,** 925–934.
Parnes, R. (1984). On singularities due to a concentrated pressure loading of a cylindrical cavity. *Int. J. Solids Structures* **20,** 267–276.
Parnes, R. (1986). Steady-state ring load pressure on a borehole surface. *Int. J. Solids Structures* **22,** 73–86.
Payton, R. G. (1983). *Elastic Wave Propagation in Transversely Isotropic Media*, Martinus, Nijhoff, The Netherlands.
Selvadurai, A. P. S. and Rajapakse, R. K. N. D. (1985). On the load transfer from a rigid cylindrical inclusion into an elastic half space. *Int. J. Solids Structures* **21,** 1213–1229.
Sendeckyj, G. P. (1974). *Mechanics of Composite Materials*, Academic Press, New York.
Sneddon, I. N. (1951). *Fourier Transforms*, McGraw-Hill, New York.
Timoshenko, S. P. and Goodier, J. N. (1970). *Theory of Elasticity*, McGraw-Hill, New York.
Wang, Y. (1992). Fundamental solutions for a multilayered transversely isotropic elastic half space and boundary element applications. Ph. D. thesis, University of Manitoba, Canada.
Williams, M. L. (1952). Stress singularities resulting from various boundary conditions in angular corners of plates in extension. *J. Appl. Mech.* **19,** 526–530.
Wong, R. (1989). *Asymptotic Approximations of Integrals*, Academic Press Inc., California.